The Astrophysical Journal, 619:L7–L10, 2005 January 20

THE ON-ORBIT PERFORMANCE OF THE *GALAXY EVOLUTION EXPLORER*

Patrick Morrissey,[1] David Schiminovich,[1] Tom A. Barlow,[1] D. Christopher Martin,[1] Brian Blakkolb,[2] Tim Conrow,[1] Brian Cooke,[2] Kerry Erickson,[2] James Fanson,[2] Peter G. Friedman,[1] Robert Grange,[3] Patrick N. Jelinsky,[4] Siu-Chun Lee,[2] Dankai Liu,[2] Alan Mazer,[2] Ryan McLean,[1] Bruno Milliard,[3] David Randall,[2] Wes Schmitigal,[2] Amit Sen,[2] Oswald H. W. Siegmund,[4] Frank Surber,[2] Arthur Vaughan,[2] Maurice Viton,[3] Barry Y. Welsh,[4] Luciana Bianchi,[5] Yong-Ik Byun,[6] Jose Donas,[3] Karl Forster,[1] Timothy M. Heckman,[5] Young-Wook Lee,[2] Barry F. Madore,[7,8] Roger F. Malina,[3] Susan G. Neff,[9] R. Michael Rich,[10] Todd Small,[1] Alex S. Szalay,[5] and Ted K. Wyder[1]

Received 2004 May 3; accepted 2004 July 27; published 2005 January 17

ABSTRACT

We report the first year's on-orbit performance results for the *Galaxy Evolution Explorer* (*GALEX*), a NASA Small Explorer that is performing a survey of the sky in two ultraviolet bands. The instrument comprises a 50 cm diameter modified Ritchey-Chrétien telescope with a 1.°25 field of view, selectable imaging and objective-grism spectroscopic modes, and an innovative optical system with a thin-film multilayer dichroic beam splitter that enables simultaneous imaging by a pair of photon-counting, microchannel-plate, delay-line readout detectors. Initial measurements demonstrate that *GALEX* is performing well, meeting its requirements for resolution, efficiency, astrometry, bandpass definition, and survey sensitivity.

Subject headings: space vehicles: instruments — surveys — telescopes — ultraviolet: general

1. INTRODUCTION

The *Galaxy Evolution Explorer* (*GALEX*) is a NASA Small Explorer mission currently performing an all-sky ultraviolet survey in two bands. *GALEX* was launched on an Orbital Sciences Corporation Pegasus rocket on 2003 April 28 at 12:00 UT from the Kennedy Space Center into a circular, 700 km, 29° inclination orbit. The instrument is designed to image a very wide 1.°25 field of view with 4″–6″ resolution and sensitivity down to an AB magnitude of $m_{\rm AB} \sim 25$ in the deepest modes.

GALEX makes science observations on the night side of each orbit during "eclipses" that are typically in the range of 1500–1800 s. In the first year of operations, we have observed over 4000 square degrees of sky and accumulated nearly a terabyte of science data. The science mission is described in a companion paper by Martin et al. (2005).

2. INSTRUMENT OVERVIEW

The instrument, shown in Figure 1, comprises a 50 cm diameter modified Ritchey-Chrétien telescope with two photon-counting, microchannel-plate (MCP), delay-line readout detectors that image the sky simultaneously in the near- and far-ultraviolet (NUV and FUV).

An optical-wheel mechanism behind the primary mirror allows selection of an imaging window, dispersive grism, or opaque shutter. Downstream of the optical wheel, a multilayer-coated dichroic beam splitter enables simultaneous imaging in the two bands. A blue-edge multilayer filter blocks geocoronal Lyα (1216 Å) and O I λ1304 emission from the FUV channel, while a red-blocking fold mirror reduces contamination from zodiacal light ($\lambda > 3000$ Å) in the NUV band. Details of the optical design are provided in Table 1.

The pair of detectors at the heart of the instrument are each completely sealed tubes with no active pumping (Jelinsky et al. 2003). Each contains a photocathode, a stack of three MCPs, and a delay-line anode with outputs at each of four corners. The 68 mm active area (75 mm diameter) Z-stack MCPs operate at a high-voltage (HV) gain of approximately 1.5×10^7 (-6200 V FUV, -5200 V NUV), producing pulses for each incoming photon that are divided by the anode and measured at each corner to determine the photon's position, which is computed by the detector electronics and stored in a solid-state recorder for later download. The FUV detector has a MgF_2 window and an opaque CsI photocathode deposited directly on the front microchannel plate, while the NUV detector has a proximity-focused semitransparent Cs_2Te photocathode deposited on the vacuum side of its fused silica window, 300 μm from the MCP surface.

3. INSTRUMENT PERFORMANCE

The instrument was calibrated in thermal vacuum during a monthlong period in mid-2001; these data form a performance baseline for flight measurements. Resolution, background, flat field, throughput, linearity, spectral resolution, and spatial distortion were measured in several sets of thermal conditions. In some areas the ground calibration provides data not easily measurable in flight, particularly the imaging-mode bandpass and

[1] Space Astrophysics Laboratory, Mail Stop 405-47, California Institute of Technology, 1200 East California Boulevard, Pasadena, CA 91125; patrick@srl.caltech.edu.
[2] Jet Propulsion Laboratory, California Institute of Technology, 4800 Oak Grove Drive, Pasadena, CA 91109.
[3] Laboratoire d'Astrophysique de Marseille, B.P. 8, Traverse du Siphon, F-13376 Marseille Cedex 12, France.
[4] Space Sciences Laboratory, University of California, Berkeley, 7 Gauss Way, Berkeley, CA 94720.
[5] Department of Physics and Astronomy, Johns Hopkins University, 3400 North Charles Street, Baltimore, MD 21218.
[6] Center for Space Astrophysics, Yonsei University, Seoul 120-749, Korea.
[7] Observatories of the Carnegie Institution of Washington, 813 Santa Barbara Street, Pasadena, CA 91101.
[8] Infrared Processing and Analysis Center, Mail Stop 100-22, California Institute of Technology, 770 South Wilson Avenue, Pasadena, CA 91125.
[9] Laboratory for Astronomy and Solar Physics, Code 681, NASA Goddard Space Flight Center, Greenbelt, MD 20771.
[10] Department of Physics and Astronomy, UCLA, Box 951547, Los Angeles, CA 90095.

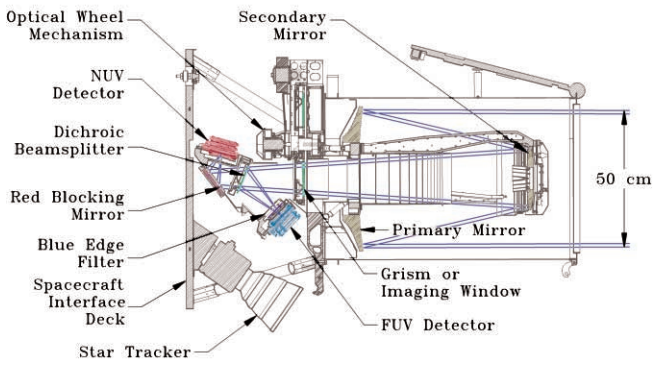

FIG. 1.—Cross section of the instrument portion of *GALEX*. The optical path is outlined in blue. Overall dimensions of the view shown are 1.5 m × 1 m. Solar panels and a separate compartment for spacecraft bus electronics (supplied by Orbital) are not included.

grism-mode dispersion. In flight, white dwarf standard stars tie the calibration to the *Hubble Space Telescope* (*HST*) system and establish the photometric zero point in each band.

To date, *GALEX* has observed six *HST* white dwarf standard stars (Bohlin et al. 2001), which span 5 magnitudes in UV intensity. Details of these observations are listed in Table 2, with key performance indicators presented in Table 3 and in the remainder of this section.

3.1. *Astrometry*

GALEX observations are dithered in a 1.′5 spiral in order to smooth out the effects of small-scale detector distortions and flat-field variations; the pipeline system must determine the spacecraft and detector transformation for each photon in the list to form sharp images. We have measured the astrometric performance against reference stars from the Tycho-2 Catalogue (Høg et al. 2000) to refine the plate solution of the instrument, with the result that 80% of stars in the central 1° of the detector area are currently found within 2.″8 of their expected location in the FUV and 1.″5 in the NUV. We expect these figures to decrease for the whole detector area as the calibration is improved with flight data.

TABLE 1

THE *GALEX* OPTICAL PRESCRIPTION

Parameter	Value
Telescope:	
Type	Ritchey-Chrétien
Coatings	MgF_2-coated Al
Primary diameter	500 mm
Secondary diameter	230 mm
Focal length	2998 mm
Focal ratio	6
Place scale	68.″80 mm^{-1}
Grism (CaF_2):	
Width (inscribed diameter)	124 mm
Thickness (center)	5.9 mm
Wedge	1.°37
Blaze angle	2.°33
Ruling	75 lines mm^{-1}
Imaging window (CaF_2):	
Diameter	124 mm
Thickness	6 mm
Dichroic (fused silica):	
Diameter	110 mm
Thickness	4 mm
Wedge	0.°119
Blue-edge filter (MgF_2):	
Diameter	74 mm
Thickness	2.5 mm
Red-blocking mirror:	
Diameter	110 mm

TABLE 2

HST WHITE DWARF STANDARDS OBSERVED BY *GALEX*

Star	m_{FUV}[a]	m_{NUV}[a]	α (J2000.0)	δ (J2000.0)
HZ 21	12.55	13.13	12 14 01.6	32 58 11.3
HZ 43	10.75	11.36	13 16 05.8	29 05 55.0
HZ 44	10.02	10.27	13 23 35.4	36 08 03.5
BD +33°2642	10.51	10.47	15 51 59.86	32 56 54.8
LDS 749B	15.57	14.71	21 32 16.3	00 15 14.4
G93-48	12.14	12.39	21 52 25.3	02 23 17.9

NOTE.—Units of right ascension are hours, minutes, and seconds, and units of declination are degrees, arcminutes, and arcseconds. Coordinates are as measured by *GALEX* and include proper motion through the 2003–2004 epoch. One exception is BD +33°2642, which was only observed in grism mode; the coordinates provided are from Bohlin et al. (2001).

[a] Magnitudes shown are predictions based on the *GALEX* bandpass and publicly available reference spectra from the *HST* CALSPEC database at http://www.stsci.edu/instruments/observatory/cdbs/calspec.html.

3.2. *Background*

The intrinsic detector background is negligible, dominated by isolated hot spots that result mainly from microscopic defects at the MCP surface. The remaining diffuse component is enhanced by a factor of 2 over the very low values observed on the ground. These results are typical for an MCP detector placed in the space radiation envronment of low Earth orbit and are consistent with little or no contribution from optics phosphorescence. More significant is the background from the sky, which varies during each eclipse by about 20%. This signal is dominated by diffuse Galactic light in the FUV and by zodiacal light in the NUV. These are orders of magnitude greater

TABLE 3

SUMMARY OF MEASURED PERFORMANCE PARAMETERS FOR *GALEX*

Item	FUV Band	NUV Band
Bandwidth[a]	1344–1786 Å	1771–2831 Å
Effective wavelength[b]	1528 Å	2271 Å
Field of view	1.°28	1.°24
Peak effective area	36.8 cm^2 at 1480 Å	61.7 cm^2 at 2200 Å
Zero point (m_0)	18.82	20.08
Image resolution	4.″5 FWHM	6.″0 FWHM
Spectral resolution ($\lambda/\Delta\lambda$)	200	90
Detector background (typical):		
Total	78 counts s^{-1}	193 counts s^{-1}
Diffuse (cm^{-2})	0.66 counts s^{-1}	1.82 counts s^{-1}
Hot spots	47 counts s^{-1}	107 counts s^{-1}
Sky background (typical)[c]	2000 counts s^{-1}	20000 counts s^{-1}
Limiting magnitude (5 σ):[d]		
AIS (100 s)	19.9	20.8
MIS (1500 s)	22.6	22.7
DIS (30000 s)	24.8	24.4
Linearity:		
Global (10% rolloff)	18000 counts s^{-1}	
Global (50% rolloff)	91000 counts s^{-1}	
Local (10% rolloff)[e]	89 counts s^{-1}	471 counts s^{-1}
Pipeline image format	3840 × 3840 elements with 1.″5 pixels	

[a] The bandpass is defined by wavelengths with effective area at least 10% of the peak.

[b] From eq. (3) of Fukugita et al. (1996).

[c] These correspond to 569 and 1189 photons s^{-1} cm^{-2} sr^{-1} $Å^{-1}$, respectively.

[d] Approximate All-sky (AIS), Medium (MIS), and Deep (DIS) Imaging Survey depths.

[e] These are worst-case values for point sources.

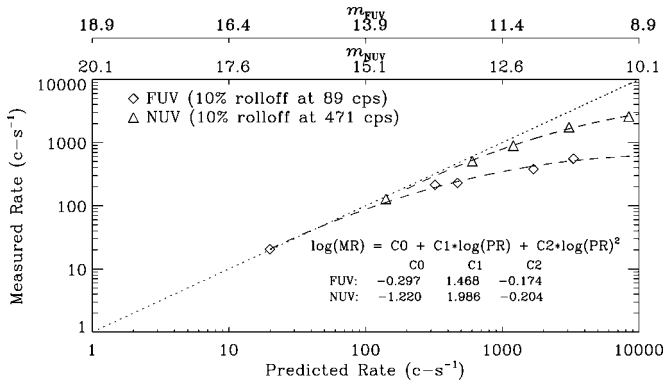

FIG. 2.—Local photometric nonlinearity measured with white dwarf standards. Empirical fits are overplotted. The function parameters PR and MR correspond to the predicted and measured source rates, respectively.

than the detector background and, along with the point-spread function (PSF), define the limiting magnitude of the deep surveys.

Other sources of background include bright-star glints in the NUV images near the edge of the detector window, large out-of-focus pupil images resulting from reflections in the imaging window and dichroic beam splitter, an arcminute-diameter skirt around bright NUV sources (at the 0.5% level) that results from the proximity-focused cathode, and photoemission from the quantum efficiency (QE) enhancing grid wires on the FUV detector window, which appear as linear features around bright sources. Work is being done to flag these locations automatically in the pipeline software, but they amount to a very small fraction of the data ($\ll$1%).[11]

3.3. *Photometry*

GALEX uses the AB magnitude system of Oke & Gunn (1983), with the FUV and NUV magnitudes defined as follows:

$$m_{\rm UV} = m_0 - 2.5 \log f_{\rm UV}.$$

Here $f_{\rm UV}$ is the dead-time–corrected count rate for a given source *divided by the flat-field map*, which is of order 1, and m_0 is the zero point corresponding to the AB magnitude of a 1 count s^{-1} flat-field–corrected detection. There are independent relative response functions and zero points for each band. The white dwarf observations show remarkable agreement with ground-test data from 2001, with only a 10% (0.1 mag) decrease in the NUV band and essentially perfect agreement in FUV. The apparent lack of degradation (and therefore contamination) is attributable to a careful contamination-control program in conjunction with the noncryogenic MCP-based design.

Repeat observations demonstrate that the current low-resolution flat field (based on ground calibration data) is performing at a level better than ± 0.1 mag rms; however, there are some subtleties that it does not capture. Chief among these is probably the shadow caused by the QE-enhancing grid wires in the FUV detector. Some work has already been done with stacks of data from deep observations at different roll angles, and these show the grid wires and also several other details quite clearly. It is expected that incorporation of these features will improve photometry, with the most significant gains for sources with short exposures that do not execute a complete dither pattern.

[11] Examples of *GALEX* data are available at http://www.galex.caltech.edu.

3.3.1. *Count-Rate Linearity and Bright-Star Constraints*

There are essentially two sources of photometric nonlinearity in the instrument: global dead time resulting from the finite time required for the electronics to assemble photon lists, and local dead time resulting from the MCP-limited current supply to small regions around bright sources. Global dead time is a linear function of the input count rate. It is easily measured using an onboard "STIM" pulser, which electronically stimulates each detector anode with a steady, low-rate stream of electronic pulses that are imaged off the field of view. Since the real rate of STIM pulses is accurately known, the measured rate is used by the pipeline to scale the effective exposure and thus correct the global dead time for all sources in the field simultaneously. This correction is typically about 10% in the NUV band and negligible in FUV; however, it can become quite significant ($\sim$50%) for the brightest fields.

Local dead time is difficult to correct with high accuracy, since it depends on the source distribution. It affects the measured count rate and shape of individual bright sources. We have used our standard stars to estimate the local dead time in each band, as shown in Figure 2. The NUV detector is more robust to bright sources because it is proximity focused and thus presents a larger image (with lower count density) to the MCP. Note that since local photometric nonlinearity is strongly source-size dependent, the saturation shown in Figure 2 for stars is a worst-case scenario.

GALEX currently adheres to a bright-star constraint of 5000 counts s^{-1}, which corresponds to approximately 10th magnitude. This significant survey constraint is being enforced in the early stage of the mission to avoid affecting the MCP gain.

3.4. *Resolution*

The width of the PSF is defined by numerous contributors, including the optics and pipeline reconstruction; however, the detectors add a large share, particularly in the proximity-focused NUV channel. To verify the fundamental instrument performance from on-orbit data, some bright stars were analyzed individually, outside the pipeline. These results show performance that is consistent with or better than what was measured during ground tests. Currently, the pipeline system is achieving about 6.″5 FWHM in the FUV band and 7.″2 in NUV, with a broad distribution in both cases. We expect to be able to improve each of these significantly (to approximately the instrument-limited values listed in Table 3) with improvements in calibration—particularly distortion-map refinements—and aspect correction algorithms.

3.5. *Spectroscopy*

The spectroscopy mode utilizes a CaF_2 grism in the converging beam of the telescope to form simultaneous spectra of all sources in the field. In a typical image, many spectra will overlap and multiple observations with different grism angles can be combined to eliminate confusion. Some early results are presented in Figure 3 for the white dwarf standard BD +33°2642.

We combined 42 spectra taken with different roll angles and at different field positions to compute the grism response in the primary orders (first for NUV and second for FUV). There is significant response in the next higher order of each band that will eventually allow some broadening of the grism bandpass. The grism effective area for the FUV band is about 15% greater on average than the response computed on the ground,

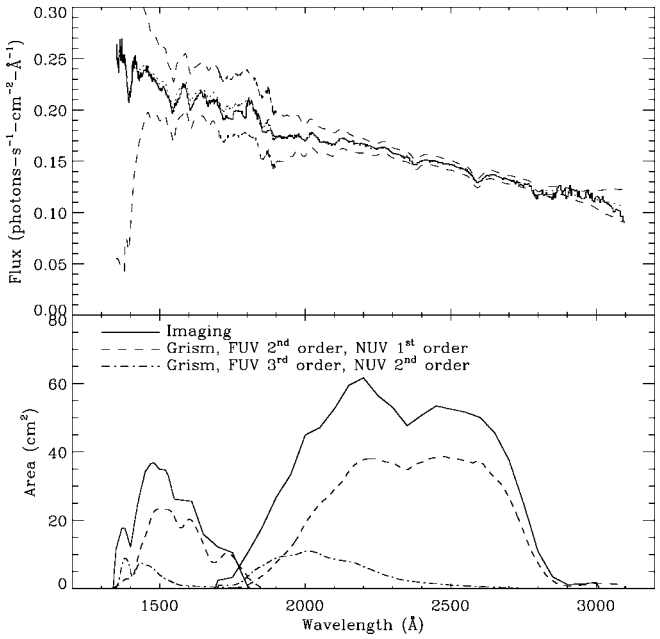

FIG. 3.—*Top*: A composite of 42 ~240 s *GALEX* spectra of the *HST* white dwarf standard star BD +33°2642 (*solid line*), the *HST* reference spectrum (*dotted line*), and the range of 1 σ variations among the 42 spectra (*dashed lines*). *Bottom*: The ground-measured imaging-mode effective area (*solid lines*), the flight-measured grism-mode effective area (*dashed lines*), and the additional effective area in the grism second (NUV) and third (FUV) orders (*dot-dashed lines*).

while the NUV band is about 10% less on average. After applying our flat-field correction, the computed grism response in the FUV varies by about 10% across the detector, and that for the NUV varies by about 3%.

The FWHM resolution derived from absorption lines in the dispersion direction is between 5″ and 6″ (~8 Å) in the FUV and 6″ and 7″ (~26 Å) in the NUV, although it may degrade toward the ends of the bandpass. The dispersion function agrees with ground-based calibrations to within a fraction of a resolution element. The offset of the spectra from the direct-mode image, which is determined by correlating extracted stars in any given field with UV stellar spectrum templates, is accurate to about 1″.

4. MISSION EFFICIENCY

Since launch, *GALEX* has had numerous detector events that are correlated with space weather. In addition to occasional HV overcurrents, which are quickly quenched by the high-speed onboard fault protection, the FUV background has jumped tens of thousands of counts per second several times and remained elevated until after a period of rest with the HV turned off. The first major example of this occurred on 2003 October 28, closely correlated with a historically large (X17) solar flare. Flight-spare laboratory tests demonstrate that charging of the front window surface enhances the detector background and that discharging the window makes the background dissipate completely. We expect our operational efficiency, currently averaging about 70%, to improve as we benefit from several flight-software patches that have addressed the space weather, window charging, and other details.

5. SUMMARY

We have reported the *GALEX* instrument performance during the first year on orbit. The satellite continues to perform well and, since it has no consumables, has the potential to continue to observe for many years. Near-term goals include improving the flight calibration to help the pipeline achieve instrument-limited performance and gradually opening the detector count-rate limits based on laboratory experiments in order to reduce bright-star constraints on survey coverage.

We gratefully acknowledge NASA's support for construction, operation, and science analysis for the *GALEX* mission, developed in cooperation with the Centre National d'Etudes Spatiales of France and the Korean Ministry of Science and Technology. The grating, window, and aspheric corrector were supplied by France. We acknowledge the dedicated team of engineers, technicians, and administrative staff from JPL/Caltech, Orbital Sciences, the University of California at Berkeley, the Laboratoire d'Astrophysique de Marseille, and the other institutions who made this mission possible.

REFERENCES

Bohlin, R. C., Dickinson, M. E., & Calzetti, D. 2001, AJ, 122, 2118
Fukugita, M., Ichikawa, T., Gunn, J. E., Doi, M., Shimasaku, K., & Schneider, D. P. 1996, AJ, 111, 1748
Høg, E., et al. 2000, A&A, 357, 367
Jelinsky, P., et al. 2003, Proc. SPIE, 4854, 233
Martin, D. C., et al. 2005, ApJ, 619, L1
Oke, J. B., & Gunn, J. E. 1983, ApJ, 266, 713